ChemPubSoc Europe

DOI: 10.1002/chem.201504995

CHEMISTRY A European Journal Full Paper

Sensors

Electrochemiluminescence of Supramolecular Nanorods and Their Application in the "On–Off–On" Detection of Copper Ions

Yan-Mei Lei, Min Zhao, Ai Wang, Yan-Qing Yu, Ya-Qin Chai, Ruo Yuan,* and Ying Zhuo*[a]

Abstract: In this work, an "on–off–on" switch system has been successfully applied through the construction of an electrochemiluminscent biosensor for copper ion (Cu^{2+}) detection based on a new electrochemiluminescence (ECL) emitter of supramolecular nanorods, which was achieved through supramolecular interactions between 3,4,9,10-perylenetetracarboxylic acid (PTCA) and aniline. The initial "signal-on" state with strong and stable ECL emission was obtained by use of the supramolecular nanorods with a new signal amplification strategy involving a co-reaction accelerator. In addition, ECL quencher probes (Fc-NH_2/Cu-Sub/nano-Au) were fabricated by immobilizing aminoferrocene (Fc-NH_2) on Cu-substrate strand modified Au nanoparticles. The quencher probes were hybridized with the immobilized Cu-enzyme strand to form Cu^{2+}-specific DNAzyme. Similarly, the "signal-off" state was obtained by the high quenching effect of Fc-NH_2 on the ECL of the excited-state PTCA (^{1}PTCA*). As expected, the second "switch-on" state could achieved by incubating with the target Cu^{2+}, owing to the Cu^{2+}-specific DNAzyme, which was irreversibly cleaved, resulting in the release of the quencher probes from the sensor interface. Herein, on the basis of the ECL intensity changes (ΔI_{ECL}) before and after incubating with the target Cu^{2+}, the prepared Cu^{2+}-specific DNAzyme-based biosensor was used for the determination of Cu^{2+} concentrations with high sensitivity, excellent selectivity, and good regeneration.

Introduction

In recent years, electrochemiluminescence (ECL) techniques have witnessed significant progress in the biosensing field because of the promises offered by the simple instrumentation required, high sensitivity, low background signal, and wide dynamic concentration response range.[1–4] Usually, ECL biosensors can be classified into two output signal modes of "signal-off" and "signal-on" strategies.[5,6] On the basis of the ECL decrease with increasing concentrations of analytes, the "signal-off" strategy has the advantages of simple steps, short operating time, and easy realization. For example, Bertoncello and his co-workers reported that the ECL emission of a CdSe@ZnS quantum dot (QD)/H_2O_2 system was quenched by glutathione to obtain the "signal-off" state.[7] However, it is generally accompanied by problems of strong background signal and "false positive or negative" errors.[8,9] Alternatively, the "signal-on" strategy, which is based on the ECL signal increase with increasing concentrations of analytes, could decrease the background signal and improve the sensitivity.[10] For instance, Zhang's group proposed that the dendrimer/CdSe–ZnS–QD nanoclusters as an ECL signal probe to get the "signal-on" state.[11] For the signal-on strategy, there is still much room for improvement of selectivity and specificity. Therefore, a more intelligent output signal mode named the "on–off–on" switch strategy was developed in recent years.[12,13] Specifically, the "on–off–on" switch contains three steps. The first step is the initial "signal-on" state with a strong signal. The second step is the "switch-off" state caused by introduction of a quencher probe. The third step is a "switch-on" state, which can be achieved in the presence of the target by taking away the quencher probe. Thus, this "on–off–on" switch strategy endows the biosensor with not only low background signal and high sensitivity, but also preferable specific recognition ability.[14]

As far as we know, the initial "signal-on" state is a prerequisite to preserve the high efficiency of the "on–off–on" ECL switch system, which can be obtained by using various signal amplification strategies, such as enzyme-based signal amplification, DNA-based signal amplification, and nanomaterial-based signal amplification.[15–17] Considering that enzymes are easily denatured and inactivated, and DNA possesses the drawbacks of high cost, easy pollution, and complex operation, nanomaterials could be an excellent candidate to circumvent these limitations. In particular, the simple, feasible, and low-cost synthetic method to achieve multi-functionalized nanomaterials has received increasing attention in recent years.[18,19,20] Supramolecular nanomaterials, which are obtained by the self-assembly method, could meet the requirements owing to their advantages of simple preparation procedures, green production, low cost, and easy large-scale production.[21–24] Known as

[a] Y.-M. Lei, Dr. M. Zhao, A. Wang, Y.-Q. Yu, Prof. Y.-Q. Chai, Prof. R. Yuan, Prof. Y. Zhuo
The Key Laboratory of Eco-environments in the Three Gorges Reservoir Region
College of Chemistry and Chemical Engineering
Southwest University, Chongqing 400715 (P.R. China)
E-mail: yuanruo@swu.edu.cn
yingzhuo@swu.edu.cn

Supporting information for this article is available on the WWW under http://dx.doi.org/10.1002/chem.201504995.

an archetype class of colorants with a large π-conjugated system, perylene and its derivatives can self-assemble to form various supramolecular nanostructures (nanowires, nanoribbons, nanorods, and nanoropes),[25–27] which exhibit a wide range of applications, including in organic electronic devices, dye lasers, fluorescent solar collectors, and optical power limiters, owing to its appealing characteristics of large specific surface area, specific optical and electronic properties, easy modification, and low manufacturing cost.[28,29] However, so far, its properties and applications in the ECL field have rarely been studied. Although we have reported the amino-terminated perylene derivative obtained by ammonolysis, which has good ECL properties, its further application was restricted owing to the disadvantages of poor film-forming ability and complicated preparation procedure.[30] Herein, new ECL supramolecular nanorods (PTCA-An) were prepared with 3,4,9,10-perylenetetracarboxylic acid (PTCA) and aniline (An) through a simple and feasible supramolecular assembly process, which not only results in large specific surface area, desirable electrical conductivity, and good membrane forming ability, but also gives a strong and stable ECL emission with a new signal amplification strategy with a co-reaction accelerator.

The other key point of the efficient "on–off–on" ECL switch system is to establish the "signal-off" state to gain the low background signal, which could be obtained by using the ECL quencher. It is well known that ferrocene (Fc) and its derivatives, as a classical quencher, have been widely applied in signal-off sensing platform construction owing to its high stability and high quenching efficiency.[31] Landers's group reported that the Fc could quench the ECL intensity of the $[Ru(bpy)_3]^{2+}$/TPrA system.[32] Ju's group demonstrated that the Fc effectively quenched the cathodic ECL of CdTe QDs.[33] Recently, the ECL quenching of Fc for the $O_2/S_2O_8^{2-}$ system has also been proven in our previous work.[34] Although Fc can act as a quencher in many ECL systems, it possesses different quenching efficiency towards different ECL systems. Thus, developing new Fc-quenched ECL systems with high quenching efficiency for the construction of signal-off sensing platforms is still desirable. Herein, we first developed a new quenching system of aminoferrocene (Fc-NH_2) for the ECL of excited-state PTCA (^{1}PTCA*), which exhibited high quenching efficiency and high signal stability.

Although copper ions (Cu^{2+}), as an essential micronutrient element, are vital to biological processes in most living organisms, its deficiency or excess can cause adverse health effects, such as liver or kidney damage, pancytopenia, and neurodegenerative diseases.[35–38] Therefore, a highly sensitive ECL biosensor based on an "on–off–on" switch strategy, combining the supramolecular nanorods of PTCA-An with the quencher of Fc-NH_2, was successfully applied for Cu^{2+} detection in this work. The first "signal-on" state was obtained by use of the PTCA-An to achieve a strong initial signal. Then, the prepared quencher probes (Fc-NH_2/Cu-Sub/nano-Au), which were obtained by the assembling the Cu-substrate (Cu-Sub) strand and Fc-NH_2 onto the surfaces of Au nanoparticles (Au NPs) by Au–N and Au–S bonds, hybridized with the Cu-Enzyme (Cu-Enz) strand to form Cu^{2+}-specific DNAzyme, resulting in effective ECL quenching to get the "signal-off" state. Finally, when the proposed biosensor was incubated with the target Cu^{2+}, the ECL signal was recovered to acquire the "signal-on" state. This could be attributed to the oxidative cleavage by the Cu^{2+}-specific DNAzyme to release the Fc-NH_2/Cu-sub/nano-Au from the sensing interface.[35] On the basis of the changes in the ECL intensities (ΔI_{ECL}) before and after incubating with the target Cu^{2+}, the prepared Cu^{2+}-specific DNAzyme biosensor was successfully applied for the determination of Cu^{2+} with high sensitivity, excellent selectivity, and good regeneration.

Experimental Section

Reagents and material

Perylene-3,4,9,10-tetracarboxylic dianhydride (PTCDA) was supplied from Lian Gang Dyestuff Chemical Industry Co. Ltd. (Liaoning, China). Hexanethiol (HT, 96%), L-ascorbic acid (AA, 99.7%), 4-(2-hydroxyethyl) piperazine-1-ethanesulfonic acid sodium salt (HEPES, 99%), sodium citrate tribasic dihydrate ($C_6H_5Na_3O_7{\cdot}2H_2O$), sodium borohydride ($NaBH_4$), and aminoferrocene (Fc-NH_2, 96%) were purchased from Sigma Chemical Co. (St. Louis, MO, USA). Hydrogen tetrachloroaurate ($HAuCl_4{\cdot}4H_2O$, 99.9%) was bought from Sinopharm Chemical Reagent Co. Ltd (Shanghai, China). $K_2S_2O_8$ was provided by Chengdu Chemical Reagent Company (Chengdu, China). Aniline (An, 99.5%) and acetone (≥99.7%) were obtained from Kelong Chemicals Inc. (Chengdu, China).

The Cu^{2+}-dependent self-cleaving DNA oligonucleotides were synthesized by Sangon Bioengineering Ltd. Company (Shanghai, China), and their sequences were as follows:

Cu-Substrate (Cu-Sub) strand:

5′-AGCTTCTTTCTAATACG**G**CTTACCCTA-$(CH_2)_6$-SH-3′ (the bold guanine indicates the cleavage site).

Cu-Enzyme(Cu-Enz) strand: 5′-SH-$(CH_2)_6$-TATCTCCACGTCGG-TAAGCCTGGGCCTCTTTCTTTTTAAGAAAGAAC-3′.

The DNA oligonucleotide samples were dissolved in 5.0 mM HEPES buffer of pH 7.0 containing 25.0 mM NaCl. Phosphate buffer solution (PBS, pH 7.4) was prepared by using 0.1 M Na_2HPO_4, 0.1 M KH_2PO_4, and 0.1 M KCl.

The colloidal Au nanoparticles (nano-Au, ≈6 nm) were prepared through the reduction of $HAuCl_4$ with sodium citrate at room temperature according to the method reported previously.[39] All other chemicals not mentioned here were of analytical reagent grade and used as received without further purification in this research. Deionized water was used throughout.

Apparatus

Fluorescence spectra were obtained with a RF-5301PC spectrophotometer (Shimadzu, Tokyo, Japan), and UV/Vis spectra were recorded on a UV-2450 UV/Vis spectrophotometer (Shimadzu, Tokyo, Japan). The measurements for cyclic voltammetry (CV) and ECL were recorded on a MPI-E multifunctional electrochemical and chemiluminescent analytical system (Xi'an Remax Electronic Science &Technology Co. Ltd., Xi'an, China). The morphologies of the supramolecular nanomaterials were characterized by using a scanning electron microscope (SEM, S-4800, Hitachi, Tokyo, Japan) at an acceleration voltage of 20–30 kV. X-ray photoelectron spectroscopy (XPS) measurements were recorded on a VG Scientific ESCALAB 250 spectrometer (Thermoelectricity Instruments, USA). All experiment were carried out with the conventional three-electrode

system containing a modified glassy carbon electrode (GCE, with diameter of 4 mm) as the working electrode, Ag/AgCl (saturated KCl) as the reference electrode, and a platinum wire as the auxiliary electrode.

Preparation the supramolecular nanorods (PTCA-An)

The supramolecular nanorods (PTCA-An) were prepared by π–π interactions and hydrogen bonding by using 3,4,9,10-perylenetetracarboxylic dianhydride (PTCDA) and aniline based on a previous report with minor modifications.[40] First, PTCDA (10 mg) was dissolved in acetone (5.0 mL), and then the aniline solution (1.0 mL, 99.5%) was added into the above solution with vigorous stirring for a week. Following that, to remove the residual acetone and An, the above admixture was centrifuged at 12000 rpm. The precipitate was washed with anhydrous ethanol and deionized water alternately until the pH was 7.4. Then, the resultant red product of PTCA-An was dispersed homogeneously in deionized water (20.0 mL) and stored in the refrigerator at 4 °C for further use.

Preparation of the quencher probes (Fc-NH_2/Cu-Sub/nano-Au)

The quencher probes of Fc-NH_2/Cu-Sub/nano-Au were achieved by the following method: First, the Cu-Sub strand (400 μL, 10 μM) with a thiol at its 3′-end was mixed with Au NPs colloidal solution (≈6 nm, 500 μL). After shaking gently for 16 h, the above admixture was centrifuged (16000 rpm, 30 min at 4 °C) to remove the excess Cu-Sub strand, and then the precipitate was dispersed in HEPES buffer (500 μL, pH 7.0) containing NaCl (25.0 mM). Subsequently, the Fc-NH_2 solution (200 μL, 100 μM) was added to the above solution with shaking overnight at room temperature to make the Fc-NH_2 immobilize on the Au NPs surface through Au–N bonding. The resultant Fc-NH_2/Cu-Sub/nano-Au probes were stored in the refrigerator at 4 °C for further use.

Fabrication of the Cu^{2+}-specific DNAzyme-based ECL biosensor

Prior to use, the GCE was polished carefully with 0.3 and 0.05 μm alumina slurry to obtain a mirror-like surface, followed by sonication in deionized water and ethanol. First, the prepared suspension of PTCA-An (5 μL) was drop cast onto the cleaned GCE surface to obtain a homogeneous film at room temperature. Subsequently, the above modified electrode (PTCA-An/GCE) was immersed in $HAuCl_4$ solution (2 mL of 1%) to obtain Au NPs by electrochemical deposition under a constant potential of −0.2 V for 40 s. After that, the Cu-Enz strand solution (15 μL, 5.0 μM; the Cu-Enz strand was heated at 95 °C for 2 min and allowed to cool to room temperature for 1 h before use) was dropped onto the above modified electrode (DepAu/PTCA-An/GCE) and kept at 4 °C for 16 h. Following that, the resultant electrode (Cu-Enz/DepAu/PTCA-An/GCE) surface was blocked with HT (15 μL, 1 mM) for 1 h at room temperature to eliminate the nonspecific binding effect. The resultant modified electrode (HT/Cu-Enz/DepAu/PTCA-An/GCE) was incubated in the quencher probe (Fc-NH_2/Cu-Sub/nano-Au) solution (15 μL) at 45 °C for 1 h. After each step, the modified electrode was thoroughly cleaned with PBS (pH 7.4) to remove the physically absorbed species. The prepared Cu^{2+}-specific DNAzyme-based ECL biosensor (Fc-NH_2/Cu-Sub/nano-Au/HT/Cu-Enz/DepAu/PTCA-An/GCE) was stored in the refrigerator at 4 °C for further use, and the corresponding schematic graph is illustrated in Scheme 1.

Measurement procedure

The prepared Cu^{2+}-specific DNAzyme-based biosensor was incubated with 10 μL of different concentrations of Cu^{2+} solution (containing 10 mM AA) at room temperature for 20 min, and then the ECL was detected by a MPI-E ECL analyzer in PBS (3 mL, 0.1 M, pH 7.4) containing $K_2S_2O_8$ (5.0 mM). The working potential was varied from −1.7 to 0 V (vs. Ag/AgCl) at a scan rate of 0.3 $V s^{-1}$ with the voltage of the photomultiplier tube (PMT) at 600 V.

Results and Discussion

SEM characterization of the different supramolecular nanomaterials

The morphologies and sizes of the as-prepared supramolecular nanomaterials were characterized by SEM. As displayed in Figure 1A, the typical SEM image of the supramolecular nanomaterial of PTCA showed a large quantity of short rod-like structures with widths of 180±30 nm and lengths of 800±200 nm, which was consistent with previous reports.[41] Compared with PTCA, the PTCA-An retained a similar rod-like shape, but its interface became more smooth and compact (Figure 1B), suggesting that the supramolecular nanorods of PTCA-An was successfully obtained by π–π interactions and hydrogen-bonds between PTCA and aniline. The UV/Vis absorption spectra of PTCA and PTCA-An are shown in Figure 1C. The maximum absorption peak of PTCA-An was located at 600 nm (Figure 1C,

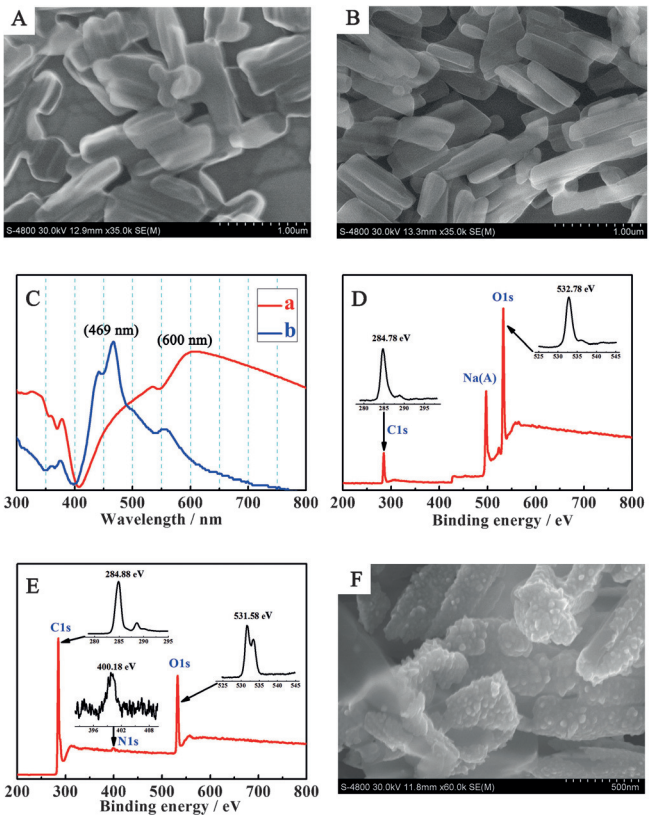

Figure 1. SEM images of PTCA (A) and PTCA-An (B). UV/Vis absorption spectrum (C) of PTCA-An (a) and PTCA (b). XPS analysis for full region of PTCA (D) and PTCA-An (E). SEM images of DepAu/PTCA-An (F).

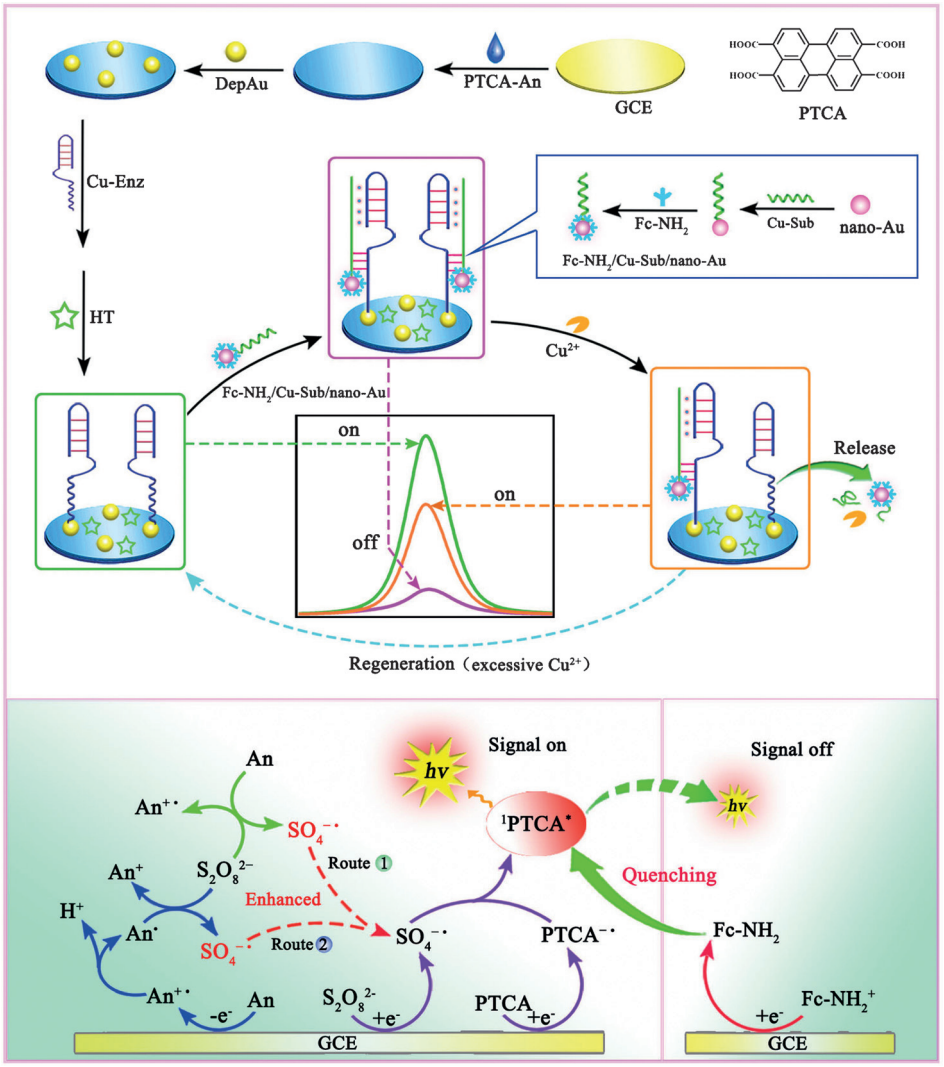

Scheme 1. Schematic illustration of the preparation procedure of the Cu^{2+}-specific DNAzyme-based ECL biosensor for Cu^{2+} detection and the possible luminescence mechanism of the "on–off–on" ECL biosensor in $S_2O_8^{2-}$ solution.

curve a), which has a clear 131 nm redshift compared with that of PTCA (469 nm: Figure 1C, curve b). These results further confirmed that stronger supramolecular interactions exist in the supramolecular nanomaterial of PTCA-An compared with that of PTCA.[42] XPS characterization (Figure 1D and E) was applied to further prove the generation of the supramolecular nanomaterials of PTCA-An. Both the O1s and C1s peaks appeared in the XPS survey spectrum of PTCA (Figure 1D) and PTCA-An (Figure 1E), whereas the N1s peaks only appeared in the XPS survey spectrum of PTCA-An. This result suggests that the supramolecular nanomaterials of PTCA-An were successfully prepared by supramolecular interactions between PTCA and An through π–π interactions and hydrogen-bonds.

Additionally, the typical SEM image of the Au NPs deposited onto the PTCA-An interface is shown in Figure 1F. It can be clearly observed that large amounts of the approximately spherical Au NPs with a diameter of approximately 50 nm were distributed uniformly and tightly on the PTCA-An surfaces, indicating that the electrodeposited generation of Au NPs allowed them to be coated successfully on the supramolecular nanorod (PTCA-An) surfaces.

ECL mechanism of the supramolecular nanorods (PTCA-An)

To investigate the ECL reaction mechanism of the supramolecular nanorods of PTCA-An, the synchronous ECL potential profiles and CV waves of the different modified electrodes were obtained in the range −1.7 to 0 V, and the results are shown in Figure 2. The bare GCE showed an evident ECL peak at −1.7 V in $S_2O_8^{2-}$ solution (Figure 2A, curve a), which could be attributed to the emission of singlet oxygen ($(^1(O_2)_2)^*$).[43] The corresponding CV wave showed a clear reduction peak at −0.75 V (Figure 2B, curve a), indicating that the sulfate radical anion ($SO_4^{-\bullet}$) was generated by reduction of $S_2O_8^{2-}$ on the electrode interface.[44] When the PTCA/GCE was measured in $S_2O_8^{2-}$ solution, an enhanced ECL signal was observed (Figure 2A, curve b). The reason may be that the co-reactant of $S_2O_8^{2-}$ reacted with the reduced species of PTCA ($PTCA^{-\bullet}$), re-

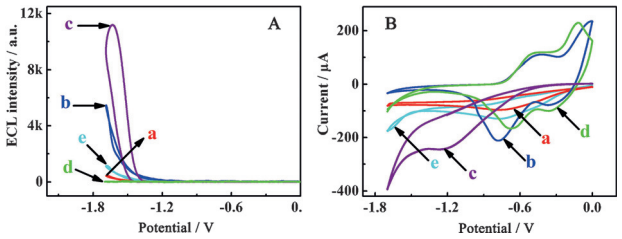

Figure 2. Synchronous ECL/potential profiles (A) and CV waves (B) for the different electrodes: bare GCE (curve a), PTCA/GCE (curve b), and PTCA-An/GCE (curve c) in $S_2O_8^{2-}$ solution, PTCA-An/GCE (curve d) in PBS solution, bare GCE in aniline + $S_2O_8^{2-}$ solution (curve e). The concentrations of $S_2O_8^{2-}$ and aniline were 0.1 M and 0.6 mM in PBS (pH 7.4), respectively.

sulting in production of the excited state of PTCA (^{1}PTCA*), which emitted light.[45] The corresponding CV wave showed an irreversible multielectron transfer process owing to the stepwise reduction process of two one-electron (1 e) transfers of PTCA, and the peak current increased owing to oxygenation between PTCA and $S_2O_8^{2-}$ (Figure 2B, curve b).[46,47] Significantly, when the PTCA-An/GCE was measured in $S_2O_8^{2-}$ solution, the ECL signal was noticeably increased about two-fold (Figure 2A, curve c) compared with that of PTCA/GCE (Figure 2A, curve b). Thus, we speculated that the aniline might act as a new co-reaction accelerator in the PTCA/$S_2O_8^{2-}$ system, which was similar to the effect of semicarbazide in the CdTe QDs/$S_2O_8^{2-}$ system.[48] Specifically, the co-reaction accelerator of aniline is a species that could interact with co-reactant of $S_2O_8^{2-}$ rather than the luminophore of PTCA to promote the ECL reaction rate of the luminophore and co-reactant, resulting in enhancement of the ECL response. Curve c in Figure 2B shows the corresponding CV wave of PTCA-An/GCE; it can be seen that the reduction peak potential shifted negatively and the corresponding peak current increased distinctly in comparison to that of PTCA/GCE (Figure 2B, curve b), indicating that the aniline could promote the oxygenation between PTCA and $S_2O_8^{2-}$. However, when the PTCA-An/GCE was measured in PBS solution, predictably, no ECL signal was observed in same potential range (Figure 2A, curve d), proving that the aniline could not interact with the luminophore (PTCA) to amplify the ECL. The corresponding CV wave exhibited two pairs of well-defined redox peaks from −1.7 V to 0 V (Figure 2B, curve d), suggesting that the supramolecular interaction between PTCA and aniline reconciled the self-derived farraginous redox peaks of PTCA successfully.[40] Subsequently, to further confirm that the aniline could promote the generation of $SO_4^{-\bullet}$, the bare GCE was measured in $S_2O_8^{2-}$ solution containing aniline, and an enhanced ECL signal was observed (Figure 2A, curve e) compared with that of bare GCE in the absence of aniline (Figure 2A, curve a). This result indicated that the aniline promoted the reduction reaction of the $S_2O_8^{2-}$ to produce more $SO_4^{-\bullet}$, which led to the production of more $^1(O_2)_2$* and the stronger emission of light. The corresponding peak current of the CV wave increased significantly in comparison to that of bare GCE in the absence of aniline (Figure 2B, curve b), further demonstrating that the aniline promoted the reduction reaction of $S_2O_8^{2-}$ to produce more $SO_4^{-\bullet}$, which thus led to the production of additional $^1(O_2)_2$* and the resulting stronger emission of

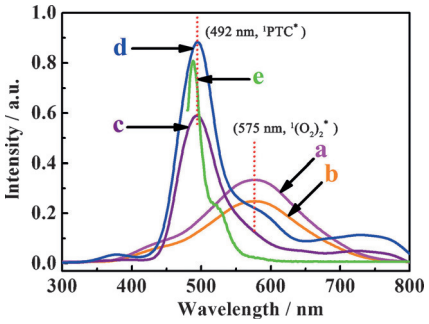

Figure 3. Normalized ECL spectrum of the bare GCE in $S_2O_8^{2-}$ solution containing aniline (a), and bare GCE (b), PTCA/GCE (c), and PTCA-An/GCE (d) in $S_2O_8^{2-}$ solution, respectively. Normalized FL spectrum of the PTCA-An solution (λ_{Ex} = 458 nm) (e).

light. That is to say, the aniline, as a new co-reaction accelerator, interacts with the co-reactant ($S_2O_8^{2-}$) rather than the luminophore (PTCA) to produce more $SO_4^{-\bullet}$, which led to generation of more ^{1}PTCA* and stronger light emission.

As shown in Figure 3, the normalized ECL spectrum was used to further investigate the ECL reaction mechanism of PTCA-An in the $S_2O_8^{2-}$ solution. The ECL spectrum of the GCE in $S_2O_8^{2-}$ solution containing aniline showed the maximum emission wavelength at 575 nm (Figure 3, curve a), which was consistent with the maximum wavelength of ECL spectrum in pure $S_2O_8^{2-}$ solution (Figure 3, curve b), confirming that the luminophore was the $^1(O_2)_2$* in $S_2O_8^{2-}$ solution. Interestingly, the ECL spectrum of PTCA/GCE in $S_2O_8^{2-}$ solution showed the maximum emission wavelength at 492 nm (Figure 3, curve c), which was consistent with the emission of PTCA-An/GCE in $S_2O_8^{2-}$ solution (Figure 3, curve d), demonstrating that the luminophore was the ^{1}PTCA* not the $^1(O_2)_2$* in $S_2O_8^{2-}$ solution. Furthermore, the fluorescence (FL) spectrum of PTCA-An (Figure 3, curve e) showed the maximum emission wavelength at 489 nm, which matched its ECL spectrum (λ_{max} = 492 nm) well, providing further evidence that the luminophore was the PTCA in $S_2O_8^{2-}$ solution because the same singlet state of ^{1}PTCA* was responsible for the emission in both cases.[46] Consequently, the possible reaction mechanism could be outlined in the following two routes:

Route 1 (homogeneous):

$$PTCA + e^- \longrightarrow PTCA^{-\bullet}$$
$$S_2O_8^{2-} + e^- \longrightarrow SO_4^{-\bullet} + SO_4^{2-}$$
$$An + S_2O_8^{2-} \longrightarrow An^{+\bullet} + SO_4^{-\bullet} + SO_4^{2-}$$
$$PTCA^{-\bullet} + SO_4^{-\bullet} \longrightarrow {}^1PTCA^* + SO_4^{2-}$$
$$^1PTCA^* \longrightarrow PTCA + h\nu$$

And route 2 (heterogeneous):

$$PTCA + e^- \longrightarrow PTCA^{-\bullet}$$
$$S_2O_8^{2-} + e^- \longrightarrow SO_4^{-\bullet} + SO_4^{2-}$$
$$An - e^- \longrightarrow An^{+\bullet}$$
$$An^{+\bullet} - H^+ \longrightarrow An^{\bullet}$$
$$S_2O_8^{2-} + An^{\bullet} \longrightarrow An^{+} + SO_4^{-\bullet}$$
$$PTCA^{-\bullet} + SO_4^{-\bullet} \longrightarrow {}^1PTCA^* + SO_4^{2-}$$
$$^1PTCA^* \longrightarrow PTCA + h\nu$$

ECL quenching mechanism between Fc-NH_2 and PTCA-An

To clarify the ECL quenching mechanism of PTCA-An by Fc-NH_2 in $S_2O_8^{2-}$ solution, the ECL intensity results over time are shown in Figure 4. Curve a in Figure 4A presents the ECL response of PTCA-An in air-saturated $S_2O_8^{2-}$ solution. It can be seen that a strong cathodic ECL emission peak, which results from the emission of ^{1}PTCA*, is located at −1.7 V with the ECL peak intensity 9033 a.u. When the Fc-NH_2 was introduced into the above detection system, the ECL intensity decreased dramatically by 63.0% (from 9033 a.u. to 3345 a.u.; Figure 4A, curve b). It could be speculated that the Fc-NH_2 could quench the ECL intensity of PTCA-An in $S_2O_8^{2-}$ solution. Significantly, when the above-modified electrode was tested in nitrogen-saturated $S_2O_8^{2-}$ solution, the ECL intensity further decreased by 86.4% (from 9033 a.u. to 1227 a.u.; Figure 4A, curve c). The reason may be that the dissolved oxygen and the ^{1}PTCA* could consume the Fc-NH_2 competitively, causing a decrease in the ECL quenching efficiency of Fc-NH_2 in air-saturated $S_2O_8^{2-}$ solution. As shown in Figure S1 (in the Supporting Information), the quenching efficiency of Fc-NH_2 was further evaluated by the quenching constant (K_{SV}) based on the ratio of the initial ECL intensity (I_0) to the intensity I at a given concentration of Fc-NH_2, following the Stern–Volmer equation:

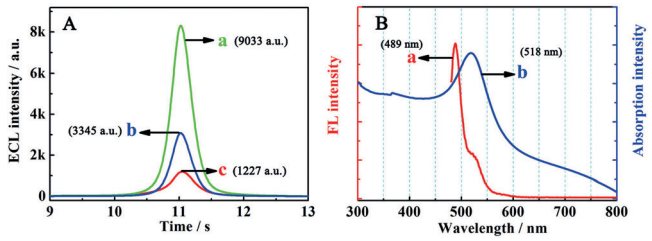

Figure 4. A) ECL intensity/time profiles of PTCA-An (a) and PTCA-An + 0.25 μM Fc-NH_2 (b) in air-saturated $S_2O_8^{2-}$ solution. (c) PTCA-An + 0.25 μM Fc-NH_2 in nitrogen-saturated $S_2O_8^{2-}$ solution. B) FL spectrum of PTCA-An (λ_{Ex} = 458 nm) (a) and UV/Vis absorption spectrum of Fc-NH_2 (b).

$$I_0/I_1 = 1 + K_{SV}[\mathrm{Fc-NH_2}]$$

in which the K_{SV} value of PTCA-An in air-saturated $S_2O_8^{2-}$ solution and nitrogen-saturated $S_2O_8^{2-}$ solution were estimated to be 6.75×10^6 M^{-1} and 2.54×10^7 M^{-1}, respectively. The FL spectrum of PTCA-An (curve a) and the UV/Vis absorption spectrum of Fc-NH_2 (curve b) are shown in Figure 4B. It can be seen that the FL spectrum of PTCA-An with the emission peak at 489 nm overlapped perfectly with the UV/Vis absorption spectrum of Fc-NH_2 with the absorbance peak at 518 nm. It could be speculated that the energy transfer would occur between Fc-NH_2 and ^{1}PTCA* in this ECL system. Herein, considering the high quenching efficiency of Fc-NH_2 on the ECL of the ^{1}PTCA*, we could presume that this ECL quenching pathway might be a synergistic effect between the energy transfer and electron transfer mechanisms.

ECL and CV characterization of the stepwise fabrication of Cu^{2+}-specific DNAzyme-based ECL biosensor

The stepwise fabrication of the Cu^{2+}-specific DNAzyme-based ECL biosensor was confirmed with ECL measurements, as shown in Figure 5A. The bare GCE exhibited a weak ECL emission peak at −1.7 V in $S_2O_8^{2-}$ solution (Figure 5A, curve a), which resulted from the transition of the excited state of $^1(O_2)_2$*. After the modification of PTCA-An on the GCE surface, a remarkable ECL response was observed (Figure 5A, curve b). The reason for this was that the luminophore of PTCA can strongly emit light, and the aniline, as a co-reaction accelerator, could further accelerate the reduction of $S_2O_8^{2-}$, resulting in the generation of more ^{1}PTCA* to emit stronger light. However, when Au NPs were electrodeposited on the electrode surface, the ECL intensity slightly decreased (Figure 5A, curve c). The reason for this may be that the hindering effect of the Au NPs between the PTCA and $S_2O_8^{2-}$ made the ECL intensity decrease slightly. After successive modification with Cu-Enz strands (Figure 5A, curve d) and HT (Figure 5A, curve e), the ECL signal further decreased sequentially owing to the insulation and steric hindrance of Cu-Enz strand and HT retarding the electron transfer on the electrode surface. When the above resultant electrode was incubated with the quencher probes (Fc-NH_2/Cu-Sub/nano-Au), the corresponding ECL intensity was sharply decreased (Figure 5A, curve f), which could be attributed to the quenching reaction between the Fc-NH_2 and the excited state of ^{1}PTCA*. Finally, after incubation with the Cu^{2+} solution (Figure 5A, curve g), the ECL emission showed significantly greater intensity than that in the absence of Cu^{2+}, which indicated that the quencher probes of Fc-NH_2/Cu-Sub/nano-Au were irreversibly self-cleaved to release the Fc-NH_2 from the electrode surface.

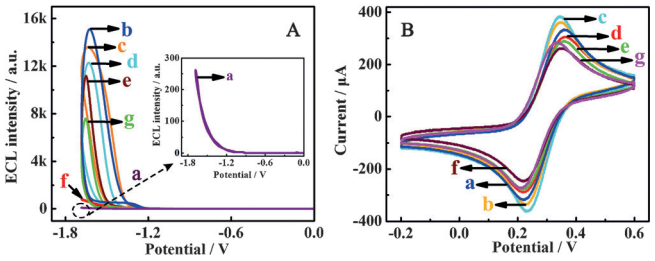

Figure 5. A) ECL responses of the electrode at different stages of functionalization in 5.0 mM $S_2O_8^{2-}$ solution (pH 7.4) and B) CV characterization of the stepwise modified electrodes performed in 0.1 M PBS (pH 7.4) containing 5.0 mM $[Fe(CN)_6]^{3-/4-}$. a) GCE, b) PTCA-An/GCE, c) DepAu/PTCA-An/GCE, d) Cu-Enz/DepAu/PTCA-An/GCE, e) HT/Cu-Enz/DepAu/PTCA-An/GCE, f) Fc-NH_2/Cu-Sub/nano-Au/HT/Cu-Enz/DepAu/PTCA-An/GCE, g,f) incubated with 1.0×10^{-7} M Cu^{2+}.

To further characterize the interfacial changes of the modified electrode at each immobilization step, cyclic voltammograms were recorded in 0.1 M PBS (pH 7.4) containing 5 mM $[Fe(CN)_6]^{3-/4-}$ (acting as the redox probe). As shown in Figure 5B, curve a exhibited a pair of well-defined redox peaks for $[Fe(CN)_6]^{3-/4-}$ on the bare GCE. When the bare GCE was modified with PTCA-An (Figure 5B, curve b) and Au NPs (Figure 5B,

curve c), the peak currents of the electrode increased sequentially because the PTCA-An and Au NPs possess excellent conductivity and large surface area to promote the electron transfer. After successive modification with Cu-Enz (Figure 5B, curve d) and HT (Figure 5B, curve e), the peak currents of the electrode decreased sequentially, indicating that the insulation and steric hindrance of the Cu-Enz strand and HT retard the electron transfer on the electrode surface. When the quencher probes of Fc-NH_2/Cu-Sub/nano-Au were modified on the electrode interface, the corresponding peak current decreased (Figure 5B, curve f). The reason for this may be that the negative charges on the electrode surface increased owing to the hybridizing reaction between Cu-Enz strands with the quencher probes of Fc-NH_2/Cu-Sub/nano-Au. As expected, the current response was greatly increased after the modified electrode was incubated with the Cu^{2+} solution, suggesting that the release of Fc-NH_2/Cu-Sub/nano-Au from the electrode surface was based on the Cu^{2+}-specific DNAzyme irreversible cleavage. The experiment results clearly demonstrated that ECL characterization was in accordance with the CV measurements.

Performance of the Cu^{2+}-specific DNAzyme-based ECL biosensor

To evaluate the sensitivity of the developed Cu^{2+}-specific DNAzyme-based ECL biosensor, experiments were performed after incubation with various concentrations of Cu^{2+} for 20 min and then ECL detection was measured in 5.0 mM $S_2O_8^{2-}$ solution (pH 7.4). As shown in Figure 6A, under the optimal conditions, the changes in the ECL intensities (ΔI_{ECL}) were found to be linearly depended on the logarithm of Cu^{2+} concentration in the range 1×10^{-12} M to 1.0×10^{-7} M. As a result, the linear regression equation was $\Delta I_{ECL}=1147.89\lg c+14351.91$ (where ΔI_{ECL} represents the change in ECL intensity and c represents the concentration of Cu^{2+}) with a correlation coefficient of $R=0.9989$ and a detection limit of 3.4×10^{-13} M (signal/noise = 3). The results demonstrated that the developed biosensor based on Cu^{2+}-specific DNAzyme was highly sensitive and has a great potential for accurate detection of Cu^{2+}. In addition, as listed in Table S1 (in the Supporting Information), the proposed biosensors were compared with other assays for the determination of Cu^{2+}. The prepared biosensor possessed good sensitivity compared with the other test platforms, indicating that it was suitable for Cu^{2+} detection at low concentrations.

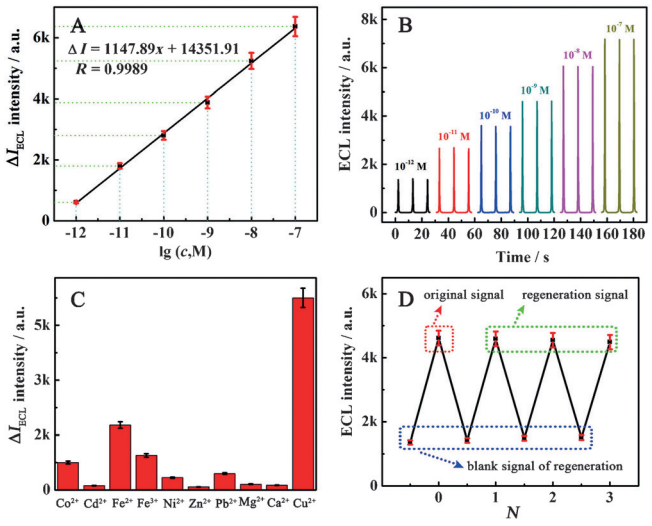

Figure 6. A) The calibration plot of the ΔI_{ECL} intensity vs. the logarithm of Cu^{2+} concentration. B) Stability of the proposed Cu^{2+}-specific DNAzyme-based ECL biosensor in various concentrations of Cu^{2+}. C) Selectivity of the prepared Cu^{2+}-specific DNAzyme-based ECL biosensor toward Cu^{2+} (1.0×10^{-9} M) by comparing it to interfering metal ions (1.0×10^{-6} M). D) Regeneration of the prepared Cu^{2+}-specific DNAzyme-based ECL biosensor incubated with target Cu^{2+} (1.0×10^{-9} M) and then hybridized with Fc-NH_2/Cu-Sub/nano-Au successively. *N* represents the number of times for the regeneration of the biosensor.

The stability of the proposed Cu^{2+}-specific DNAzyme-based ECL biosensor was demonstrated with various concentrations of Cu^{2+}. As shown in Figure 6B, the ECL intensity increased correspondingly with the increase in Cu^{2+} concentration, and stable ECL/time curves were obtained under continuous CV scanning for three cycles (with the scan range −1.7 V to 0 V and scan rate 0.3 $V s^{-1}$) in different concentration ranges (from 1×10^{-12} M to 1.0×10^{-7} M). It is seen that the prepared biosensor has good stability for Cu^{2+} detection.

The selectivity of the prepared Cu^{2+}-specific DNAzyme-based ECL biosensor for Cu^{2+} was evaluated by against other interference metal ions, including Co^{2+}, Cd^{2+}, Fe^{2+}, Fe^{3+}, Ni^{2+}, Zn^{2+}, Pb^{2+}, Mg^{2+} and Ca^{2+} at a concentration of 1.0×10^{-6} M and Cu^{2+} at 1.0×10^{-9} M. As shown in Figure 6C, Cd^{2+}, Ni^{2+}, Zn^{2+}, Pb^{2+}, Mg^{2+}, and Ca^{2+} exhibited negligible interference in the detection of Cu^{2+}. Fe^{2+}, Fe^{3+}, and Co^{2+} caused a slight ECL enhancement, but their concentrations were 1000 times as high as the target Cu^{2+}. Thus, the results suggested that the prepared biosensor exhibited a remarkably high selectivity for Cu^{2+} over other competing metal ions.

The regeneration of the prepared biosensor has been investigated for Cu^{2+} detection as shown in Figure 6D. The first ECL response of Fc-NH_2/Cu-Sub/nano-Au/HT/Cu-Enz/DepAu/PTCA-An/GCE was recorded as the blank signal of regeneration. Then, the second ECL response was recorded as the original signal after the biosensor was incubated with the target Cu^{2+} (1.0×10^{-9} M). Afterwards, when the biosensor was incubated with 1.0×10^{-3} M Cu^{2+} solution to release the residual quencher probes from the sensing interface and then incubated with the quencher probes to rebuild Fc-NH_2/Cu-Sub/nano-Au/HT/Cu-Enz/DepAu/PTCA-An/GCE, the corresponding ECL signal was recorded as the regeneration signal. This regeneration procedure was repeated three times for one Cu^{2+}-specific DNAzyme-based ECL biosensor. The relative standard deviation of these measurements was only 6.2%, indicating that the prepared biosensor has a good regeneration ability for Cu^{2+} detection.

Direct detection of Cu^{2+} in human hair

The capacity of the Cu^{2+}-specific DNAzyme-based ECL biosensor was investigated in an extraction solution of human hair (the sample pretreatment process is shown in the Supporting Information), and the results are shown in Figure S1 (in the

Supporting Information). Compared with the Cu^{2+} standard solutions (Figure S2, curve a), the calibration curve of the sample solutions exhibited an approximate slope (Figure S2, curve b), indicating that the proposed biosensor has potential applications for Cu^{2+} detection in practical samples with good accuracy and acceptable precision.

Conclusions

A new "on–off–on" switch system has been designed for the highly sensitive and selective detection of Cu^{2+} by using Fc-NH_2/Cu-Sub/nano-Au as quencher probes on a PTCA-An modified electrode. Remarkably, the PTCA-An nanorods were obtained by a simple and facile supramolecular assembly process, which not only gave a large specific surface area, desirable electrical conductivity, and good membrane forming ability, but also gave nanorods that exhibited strong and stable ECL emission based on the use of the co-reaction accelerator for boosting signal amplification. Furthermore, the quencher probes of Fc-NH_2/Cu-Sub/nano-Au showed high quenching efficiency on the ECL emission of PTCA with a low background signal. Thus, the prepared Cu^{2+}-specific DNAzyme-based ECL biosensor showed high sensitivity, excellent selectivity, and good regeneration, and thus provides a promising sensing platform for Cu^{2+} analysis in real samples.

Acknowledgments

This work was financially supported by the NNSF of China (21575116, 21275119, 51473136), and the Fundamental Research Funds for the Central Universities (XDJK2015A002, XDJK2014A012), China.

Keywords: biosensors · copper · electrochemiluminescence · supramolecular nanorods

[1] G. Valenti, M. Zangheri, S. E. Sansaloni, M. Mirasoli, A. Penicaud, A. Roda, F. Paolucci, *Chem. Eur. J.* **2015**, *21*, 12640 – 12645.
[2] L. Z. Hu, G. B. Xu, *Chem. Soc. Rev.* **2010**, *39*, 3275 – 3304.
[3] K. N. Swanick, M. Sandroni, Z. Ding, E. Zysman-Colman, *Chem. Eur. J.* **2015**, *21*, 7435 – 7440.
[4] C. Adam, A. Wallabregue, H. Li, J. Gouin, R. Vanel, S. Grass, J. Bosson, L. Bouffier, J. Lacour, N. Sojic, *Chem. Eur. J.* **2015**, *21*, 1 – 8.
[5] X. Wang, W. Yun, P. Dong, J. Zhou, P. He, Y. Fang, *Langmuir* **2008**, *24*, 2200 – 2205.
[6] C. Zhou, J. Luo, L. Zhang, Y. Long, C. Wang, D. Xiao, *J. Mater. Chem. C* **2014**, *2*, 9949 – 9956.
[7] L. Dennany, M. Gerlach, S. O'Carroll, T. E. Keyes, R. J. Forster, P. Bertoncello, *J. Mater. Chem.* **2011**, *21*, 13984 – 13990.
[8] X. F. Wang, Y. Zhou, J. J. Xu, H. Y. Chen, *Adv. Funct. Mater.* **2009**, *19*, 1444 – 1450.
[9] J. Zhang, P. Chen, X. Wu, J. Chen, L. Xu, G. Chen, F. Fu, *Biosens. Bioelectron.* **2011**, *26*, 2645 – 2650.
[10] Z. Liu, W. Zhang, L. Hu, H. Li, S. Zhu, G. Xu, *Chem. Eur. J.* **2010**, *16*, 13356 – 13359.
[11] G. Jie, L. Wang, J. Yuan, S. Zhang, *Anal. Chem.* **2011**, *83*, 3873 – 3880.
[12] L. Deng, Y. Du, J. J. Xu, H. Y. Chen, *Biosens. Bioelectron.* **2014**, *59*, 58 – 63.
[13] Y. T. Liu, J. P. Lei, Y. Huang, H. X. Ju, *Anal. Chem.* **2014**, *86*, 8735 – 8741.
[14] X. Du, D. Jiang, N. Hao, Q. Liu, J. Qian, L. Dai, H. Mao, K. Wang, *Chem. Commun.* **2015**, *51*, 11236 – 11239.
[15] J. J. Li, Y. Chu, B. Y. H. Lee, X. S. Xie, *Nucleic Acids Res.* **2008**, *36*, e36.
[16] J. Wang, G. Liu, B. Munge, L. Lin, Q. Zhu, *Angew. Chem. Int. Ed.* **2004**, *43*, 2158 – 2161; *Angew. Chem.* **2004**, *116*, 2210 – 2213.
[17] Q. Xu, F. Yan, J. Lei, C. Leng, H. Ju, *Chem. Eur. J.* **2012**, *18*, 4994 – 4998.
[18] Q. Lin, X. Huang, J. Tang, Y. Han, H. J. Chen, *J. Nanopart. Res.* **2013**, *15*, 1 – 7.
[19] J. Han, Y. Zhuo, Y. Chai, R. Yuan, W. Zhang, Q. Zhu, *Anal. Chim. Acta* **2012**, *746*, 70 – 76.
[20] J. J. Xu, W. W. Zhao, S. Song, C. Fan, H. Y. Chen, *Chem. Soc. Rev.* **2014**, *43*, 1601 – 1611.
[21] E. Busseron, Y. Ruff, E. Moulin, N. Giuseppone, *Nanoscale* **2013**, *5*, 7098 – 7140.
[22] F. Würthner, T. E. Kaiser, C. R. Saha-Möller, *Angew. Chem. Int. Ed.* **2011**, *50*, 3376 – 3410; *Angew. Chem.* **2011**, *123*, 3436 – 3473.
[23] D. González-Rodríguez, A. P. Schenning, *Chem. Mater.* **2010**, *22*, 310 – 325.
[24] B. Rybtchinski, *ACS Nano* **2011**, *5*, 6791 – 6818.
[25] Y. Huang, J. Hu, W. Kuang, Z. Wei, C. F. Faul, *Chem. Commun.* **2011**, *47*, 5554 – 5556.
[26] Y. Liu, K. R. Wang, D. S. Guo, B. P. Jiang, *Adv. Funct. Mater.* **2009**, *19*, 2230 – 2235.
[27] S. Yagai, Y. Monma, N. Kawauchi, T. Karatsu, A. Kitamura, *Org. Lett.* **2007**, *9*, 1137 – 1140.
[28] C. Huang, S. Barlow, S. R. Marder, *J. Org. Chem.* **2011**, *76*, 2386 – 2407.
[29] R. A. Cormier, B. A. Gregg, *Chem. Mater.* **1998**, *10*, 1309 – 1319.
[30] Y. M. Lei, W. X. Huang, M. Zhao, Y. Q. Chai, R. Yuan, Y. Zhuo, *Anal. Chem.* **2015**, *87*, 7787 – 7794.
[31] S. Fery-Forgues, B. Delavaux-Nicot, *J. Photochem. Photobiol. A* **2000**, *132*, 137 – 159.
[32] W. Cao, J. P. Ferrance, J. Demas, J. P. Landers, *J. Am. Chem. Soc.* **2006**, *128*, 7572 – 7578.
[33] S. Deng, J. Lei, Y. Liu, Y. Huang, H. Ju, *Chem. Commun.* **2013**, *49*, 2106 – 2108.
[34] Y. Zhuo, J. Han, L. Tang, N. Liao, G. F. Gui, Y. Q. Chai, R. Yuan, *Sens. Actuators B* **2014**, *192*, 791 – 795.
[35] J. L. He, S. L. Zhu, P. Wu, P. P. Li, T. Li, Z. Cao, *Biosens. Bioelectron.* **2014**, *60*, 112 – 117.
[36] J. Liu, Y. Lu, *J. Am. Chem. Soc.* **2007**, *129*, 9838 – 9839.
[37] C. Ge, Q. Luo, D. Wang, S. Zhao, X. Liang, L. Yu, X. Xing, L. Zeng, *Anal. Chem.* **2014**, *86*, 6387 – 6392.
[38] M. Nguyen, A. Robert, A. Sournia-Saquet, L. Vendier, B. Meunier, *Chem. Eur. J.* **2014**, *20*, 6771 – 6785.
[39] K. R. Brown, A. P. Fox, M. J. Natan, *J. Am. Chem. Soc.* **1996**, *118*, 1154 – 1157.
[40] Y. Y. Chang, S. B. Xie, Y. Q. Chai, Y. L. Yuan, R. Yuan, *Chem. Commun.* **2015**, *51*, 7657 – 7660.
[41] Y. Yuan, R. Yuan, Y. Chai, Y. Zhuo, X. Gan, L. Bai, *Chem. Eur. J.* **2012**, *18*, 14186 – 14191.
[42] K. Balakrishnan, A. Datar, T. Naddo, J. Huang, R. Oitker, M. Yen, L. Zang, *J. Am. Chem. Soc.* **2006**, *128*, 7390 – 7398.
[43] E. P. Koval'chuk, O. V. Reshetnyak, A. O. Chernyak, Y. S. Kovalyshyn, *Electrochim. Acta* **1999**, *44*, 4079 – 4086.
[44] D. Jiang, X. Du, Q. Liu, L. Zhou, J. Qian, K. Wang, *ACS Appl. Mater. Interfaces* **2015**, *7*, 3093 – 3100.
[45] J. Suk, Z. Wu, L. Wang, A. J. Bard, *J. Am. Chem. Soc.* **2011**, *133*, 14675 – 14685.
[46] S. K. Lee, Y. Zu, A. Herrmann, Y. Geerts, K. Müllen, A. J. Bard, *J. Am. Chem. Soc.* **1999**, *121*, 3513 – 3520.
[47] E. F. Fabrizio, I. Prieto, A. J. Bard, *J. Am. Chem. Soc.* **2000**, *122*, 4996 – 4997.
[48] M. N. Ma, Y. Zhuo, R. Yuan, Y. Chai, *Anal. Chem.* **2015**, *87*, 11389 – 11397.

Received: December 11, 2015
Revised: March 16, 2016
Published online on May 3, 2016